

Deformation of a Peregrine soliton by fluctuating backgrounds

H. J. Shin*

Department of Physics and Research Institute of Basic Sciences, Kyung Hee University, Seoul 130-701, Korea

(Received 30 May 2013; revised manuscript received 29 August 2013; published 30 September 2013)

A generalized Peregrine soliton moving on a fluctuating background is constructed. The agreement with the experimental results is improved compared to the standard Peregrine soliton. It has a deformed shape asymmetric with respect to time, and the peak values are not always 3.

DOI: [10.1103/PhysRevE.88.032919](https://doi.org/10.1103/PhysRevE.88.032919)

PACS number(s): 05.45.Yv, 47.35.Fg, 42.65.Tg

I. INTRODUCTION

The Peregrine soliton [1] models the rogue wave [2] based on nonlinear dynamics. It is a solution of the nonlinear Schrödinger equation (NLSE), localized both in space and time. It has a large-amplitude peak of 3 above the background wave [3]. Recent studies realized the Peregrine solitons in various areas of physics, including in fiber optics [4], in a water wave [5,6], and in multicomponent plasma [7].

Figure 1 (solid line) shows a rogue wave produced in a $15\text{ m} \times 1.6\text{ m} \times 1.5\text{ m}$ water tank with 1 m water depth [5]. A single-flap paddle located at one end of the tank is displaced according to the surface height of the Peregrine soliton and provides the proper initial condition. The experimental results (solid line) were very close to the analytic predictions from the standard Peregrine soliton (dotted line). However, we can see some asymmetry in the surface elevation with respect to time in Fig. 1. There also appears a small fluctuation of the amplitude of the background wave. These small discrepancies between the experiments and theories seem ubiquitous in rogue wave phenomena. They could be generated by various causes, for example, by the irregular motion of the paddle in providing the initial condition. Similar types of discrepancies between the theories and experiments are observed in [6,7].

Motivated by the above observations, we will construct a generalized Peregrine soliton (dashed line). It has asymmetry in time and resides on a fluctuating background. It can describe the rogue wave observed in a water tank more correctly than the standard Peregrine soliton.

II. FORMULATION

Deep water waves are described by the following nonlinear equation [8]:

$$i\left(\frac{\partial a}{\partial t} + c_g \frac{\partial a}{\partial x}\right) - \frac{\omega_0}{8k_0^2} \frac{\partial^2 a}{\partial x^2} - \frac{\omega_0 k_0^2}{2} |a|^2 a = 0, \quad (1)$$

where t and x are time and longitudinal coordinates. The wave number k_0 and the frequency of the carrier wave ω_0 satisfy the dispersion relation of the linear deep water wave, $\omega_0 = \sqrt{gk_0}$, with the gravitational acceleration g . The group

velocity is $c_g = \frac{d\omega}{dk_0} = \frac{\omega_0}{2k_0}$. Then the surface elevation $\eta(x, t)$ is given by

$$\eta(x, t) = \text{Re}\{a(x, t)\exp[i(k_0 x - \omega_0 t)]\}. \quad (2)$$

The solution of Eq. (1) can be obtained from that of the following standard NLSE:

$$i\bar{\partial}\psi + \partial^2\psi + 2|\psi|^2\psi = 0 \quad (3)$$

by substituting

$$\bar{z} = -\frac{k_0^2 a_0^2 \omega_0}{4} t, \quad z = \sqrt{2} k_0 a_0 (x - c_g t),$$

$$\psi(z, \bar{z}) = a(x, t)/a_0 \quad (4)$$

($\partial \equiv \frac{\partial}{\partial z}, \bar{\partial} \equiv \frac{\partial}{\partial \bar{z}}$). One should note that \bar{z} is the rescaled variable of time and is *not* complex conjugate to z , which is the rescaled variable of coordinate. We use the notation $\psi_0(z, \bar{z})^*$ to denote the complex conjugation of $\psi_0(z, \bar{z})$ as in Eq. (7).

We generalize the Peregrine soliton such that it is a localized solution lying on a fluctuating background $\psi_0(z, \bar{z})$ such that

$$\psi_0(z, \bar{z}) = -i [1 + \epsilon \cos Y] e^{2i\bar{z} - i\epsilon \frac{\sigma}{\Omega^2} \sin Y}, \quad (5)$$

where

$$Y = \Omega z + \sigma \bar{z} + \theta, \quad \sigma = \pm \Omega \sqrt{\Omega^2 - 4}, \quad (6)$$

and Ω, θ are arbitrary parameters. $\psi_0(z, \bar{z})$ is an approximate solution up to order $O(\epsilon^1)$ of the NLSE (3). There occurs a modulational instability for ψ_0 for $2 > \Omega > -2$, and we should take $|\Omega| \geq 2$ [9,10]. (When a modulational instability occurs, it is difficult to observe a rogue wave lying on this type of background. This case includes the higher order rogue waves.) In the present work, we take $\Omega \approx 2$, which shows distinctive features of the fluctuating backgrounds without invoking the instability.

III. DERIVATION OF THE ROGUE WAVE WITH FLUCTUATING BACKGROUND

To obtain a superposed solution of a rogue wave plus a fluctuating background using the Darboux transformation, we first need to find a solution for $\psi_i, i = 1, 2$, of the

*hjshin@khu.ac.kr

following associated linear equation (Lax pair):

$$\begin{aligned} \partial \begin{pmatrix} \psi_1 \\ \psi_2 \end{pmatrix} &= \begin{pmatrix} -i\lambda & i\psi_0(z, \bar{z}) \\ i\psi_0(z, \bar{z})^* & i\lambda \end{pmatrix} \begin{pmatrix} \psi_1 \\ \psi_2 \end{pmatrix}, \\ \bar{\partial} \begin{pmatrix} \psi_1 \\ \psi_2 \end{pmatrix} &= \begin{pmatrix} -2i\lambda^2 + i|\psi_0(z, \bar{z})|^2 & 2i\lambda\psi_0(z, \bar{z}) - \partial\psi_0(z, \bar{z}) \\ 2i\lambda\psi_0(z, \bar{z})^* + \partial\psi_0(z, \bar{z})^* & 2i\lambda^2 - i|\psi_0(z, \bar{z})|^2 \end{pmatrix} \begin{pmatrix} \psi_1 \\ \psi_2 \end{pmatrix}. \end{aligned} \quad (7)$$

A. Solution of Eq. (7) from the modified squared wave function approach

A general solution of Eq. (7) was constructed in [11,12] using the modified squared wave function approach. It is expressed in terms of four parameters, V_0, A, k, λ , as follows:

$$\begin{aligned} \psi_0(z, \bar{z}) &= -i\sqrt{v_0}e^{i\beta_0\bar{z}+i\phi_0(z)}, \\ \psi_i(z, \bar{z}) &= \sqrt{v_i}e^{i\beta_i\bar{z}+i\phi_i(z)}, \quad i = 1, 2, \end{aligned} \quad (8)$$

where

$$\begin{aligned} v_i &= V_i + A^2\text{cn}^2(\kappa z, k), \quad i = 0, 1, 2, \\ \phi_0(z) &= \int \frac{C_0}{v_0} dz, \quad \phi_i(z) = \int \frac{C_i}{v_i} dz \pm \lambda z, \quad i = 1, 2, \end{aligned} \quad (9)$$

with $\kappa^2 = A^2/k^2$ and

$$\begin{aligned} V_i &= \kappa^2/2 - V_0/2 - A^2 - 2\lambda^2 \pm 2\sqrt{P}, \quad i = 1, 2, \\ \beta_0 &= -\kappa^2 + 3V_0 + 2A^2, \quad \beta_i = \pm\beta_0/2 + 2\sqrt{P}, \quad i = 1, 2, \\ C_0 &= -\sqrt{-V_0(V_0 + A^2)(V_0 + A^2 - \kappa^2)}, \\ C_i &= \pm 4\lambda(\lambda^2 + \beta_0/4 \mp \sqrt{P}) \mp C_0, \quad i = 1, 2, \\ P &= \lambda^4 + \frac{\beta_0}{2}\lambda^2 - C_0\lambda + (\kappa^2 - A^2 - V_0) \\ &\quad \times (\kappa^2 + A^2 + 3V_0)/16 + A^4/16, \end{aligned} \quad (10)$$

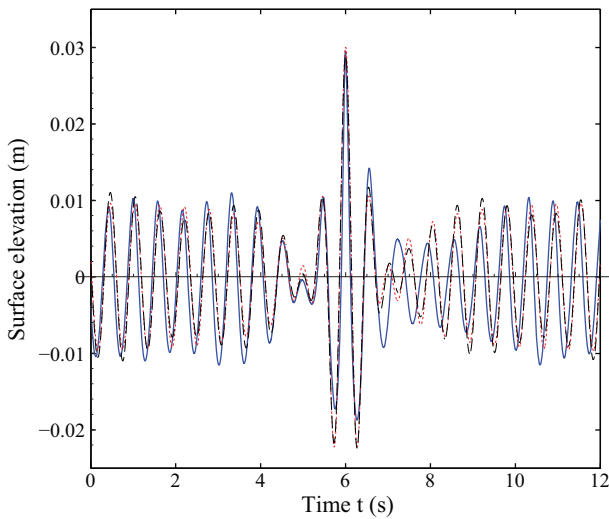


FIG. 1. (Color online) Comparison of measured surface height at the position of maximum rogue wave amplitude (solid blue line) with the theoretical standard Peregrine solution (dotted red line) and the generalized Peregrine solution (dashed black line), adapted from Chabchoub *et al.* [5]. Copyright 2011 by the American Physical Society.

where the upper sign is for $i = 1$ while the lower sign is for $i = 2$ in \pm and \mp symbols. Here cn is the standard Jacobi elliptic functions, and $k \in (0, 1)$ is the modulus of the Jacobi function.

B. Specific limit of Eq. (8) for the rogue wave

To obtain a solution corresponding to the generalized Peregrine soliton of a rogue wave plus a fluctuating background, we need to take a specific limit on λ in the solution in Eq. (8). (General λ values give the standard soliton on a fluctuating background; see more details in [11].) The key observation of the present paper is in taking the limit on λ such that $P \rightarrow 0$. Then the $O(\sqrt{P})$ term in the series expansion of $\psi_i, i = 1, 2$ with respect to \sqrt{P} gives

$$\begin{aligned} \psi_i &= \sqrt{S(z)} \left(\pm \frac{1}{S(z)} + 2i\bar{z} - 4i\lambda \int \frac{dz}{S(z)} - 2iC_p \int \frac{dz}{S(z)^2} \right) \\ &\quad \times e^{\pm i\beta_0\bar{z}/2 \pm i\lambda z \pm iC_p \int \frac{dz}{S(z)}}, \quad i = 1, 2, \end{aligned} \quad (11)$$

where

$$\begin{aligned} S(z) &= \kappa^2/2 - V_0/2 - A^2 - 2\lambda^2 + A^2\text{cn}^2(\kappa z, k), \\ C_p &= 4\lambda(\lambda^2 + \beta_0/4) - C_0, \end{aligned} \quad (12)$$

and λ is a solution of $P = 0$ in Eq. (10). ψ_0 remains unchanged as in Eq. (8), and this new set $\psi_i, i = 0, 1, 2$, is a solution of the linear equation in Eq. (7) with three parameters, V_0, A , and κ , with $k^2 = A^2/\kappa^2$.

C. Specific limit of Eqs. (8) and (11) for a small fluctuating background

Now by taking a limit on the three parameters in Eqs. (8) and (11) such that

$$V_0 = 1 - 2\epsilon, \quad A^2 = 4\epsilon, \quad \kappa = \frac{\Omega}{2} + \frac{2}{\Omega}\epsilon, \quad (13)$$

with $\epsilon \rightarrow 0$, we can obtain a solution which can describe the Peregrine soliton on a small fluctuating background. Explicitly, the solution which satisfies the associated linear equation (7) up to $O(\epsilon^1)$ is (we multiply an irrelevant factor $\sqrt{2\Delta}$ to ψ_1, ψ_2)

$$\begin{aligned} \psi_0 &= -i(1 + \epsilon \cos \Omega z) \exp \left[i \left(3 - \frac{\Omega^2}{4} \right) \bar{z} \right. \\ &\quad \left. - i\eta \left(z - \frac{2\epsilon}{\Omega} \sin \Omega z \right) \right], \end{aligned}$$

$$\psi_i = \left[\pm 1 - 2z + 4i\Delta\bar{z} - \frac{\epsilon}{2\Delta}(\mp 1 - 2z + 4i\Delta\bar{z})\cos\Omega z - \frac{2i\epsilon\eta}{\Delta\Omega}\sin\Omega z \right] \exp\left[\pm i\left(\frac{3}{2} - \frac{\Omega^2}{8}\right)\bar{z} \mp i\frac{\eta}{2}z \pm \frac{\epsilon}{\Omega}\sin\Omega z\right], \quad i = 1, 2, \quad (14)$$

with

$$\lambda = -i + \frac{\eta}{2}, \quad (15)$$

where

$$\eta = \sqrt{\frac{\Omega^2}{4} - 1}, \quad \Delta = 1 + i\sqrt{\frac{\Omega^2}{4} - 1}. \quad (16)$$

By inserting Eqs. (13) and (15) into P in Eq. (10), we can find $P = 0$ up to $O(\epsilon^1)$ (the rogue wave condition in Sec. III B). Equation (14) has two parameters, Ω and ϵ , and has the merit of being expressed in terms of the elementary functions.

D. Solution of Eq. (7) for the rogue wave with a fluctuating background

Finally, by replacing the variable in the trigonometric functions as $\Omega z \rightarrow \Omega z + \sigma\bar{z} + \theta$ and adjusting the phase of the exponential factor, we can obtain the solution ψ_0 in Eq. (5) instead of ψ_0 in Eq. (14). Similarly, we obtain ψ_1, ψ_2 as follows [instead of those in Eq. (14)]:

$$\begin{aligned} \psi_1 &= \left[1 - 2z + 4i\bar{z} - \frac{\epsilon\Omega}{2\Omega - i\sigma}(1 + 2z - 4i\bar{z})\cos Y + \frac{2i\epsilon\sigma}{\Omega(2\Omega - i\sigma)}\sin Y \right] e^{i\bar{z} + \frac{\epsilon}{\Omega}\sin Y}, \\ \psi_2 &= \left[-1 - 2z + 4i\bar{z} - \frac{\epsilon\Omega}{2\Omega - i\sigma}(-1 + 2z - 4i\bar{z})\cos Y + \frac{2i\epsilon\sigma}{\Omega(2\Omega - i\sigma)}\sin Y \right] e^{-i\bar{z} - \frac{\epsilon}{\Omega}\sin Y}. \end{aligned} \quad (17)$$

ψ_0 in Eq. (5) and ψ_1, ψ_2 in Eq. (17) satisfy the associated linear equation (7) up to $O(\epsilon^1)$ with

$$\lambda = -i. \quad (18)$$

As the solution in Eq. (17) is crucial in obtaining the generalized Peregrine soliton, we check the solution using MATHEMATICA by explicitly substituting $\lambda, \psi_0, \psi_1, \psi_2$ into Eq. (7). We note that the modified squared wave function approach can provide a more generalized form of solution than those in Eq. (8), which has five parameters. Starting from this more generalized solution, we can obtain the solution in Eq. (17) directly without the need of above variables replacement procedure.

E. Peregrine soliton with a small fluctuating background

Then, a generalized Peregrine soliton ψ^{r-c} (a rogue wave plus a fluctuating background) is constructed using the Darboux transformation [13] [it is correct up to $O(\epsilon^1)$]:

$$\begin{aligned} \psi^{r-c}(z, \bar{z}) &= \psi_0(z, \bar{z}) - 2(\lambda - \lambda^*) \left(\frac{\psi_2}{\psi_1} + \frac{\psi_1^*}{\psi_2^*} \right)^{-1} \\ &= i e^{2i\bar{z}} \left[1 - \epsilon \cos Y + i\epsilon \frac{\sigma}{\Omega^2} \sin Y - \frac{4 + 16i\bar{z} - \epsilon \frac{16}{\Omega^2} (\cos Y + \Omega z \sin Y) - i\epsilon\sigma \frac{16}{\Omega^4} (\Omega z \cos Y - \sin Y)}{1 - \epsilon \frac{4}{\Omega^2} \cos Y + (4z^2 + 16\bar{z}^2)(1 + \epsilon \frac{4}{\Omega^2} \cos Y) - \epsilon \frac{32}{\Omega^4} (\Omega z - \sigma\bar{z}) \sin Y} \right]. \end{aligned} \quad (19)$$

The Darboux transformation guarantees the correctness of the solution in Eq. (19) when ψ_0, ψ_1, ψ_2 satisfies the linear equation in Eq. (7). A direct check of the solution in Eq. (19) is accomplished by using MATHEMATICA. The solution was plugged back into the NLSE and satisfies it up to $O(\epsilon^1)$.

IV. DISCUSSION

Figure 2(a) shows the standard Peregrine soliton which is obtained by taking $\epsilon = 0$ in Eq. (19). Figure 2(b) shows a generalized Peregrine soliton lying on a fluctuating background. It is obtained from Eq. (19) with the parameters $\epsilon = 0.15, \Omega = 2.3$ (thus $\sigma = 2.61$), and $\theta = -3\pi/4$.

The plot in Fig. 2(a) (standard Peregrine soliton) has a peak value of 3 at $z = \bar{z} = 0$. On the other hand, the peak values of the generalized Peregrine solitons are different from 3. For example, when $\Omega = 2.3, \epsilon = 0.15, \theta = -3\pi/4$, the peak value of $|\psi^{r-c}|$ is 2.913 and occurs at $z = -0.0018, \bar{z} = 0.033$, while $|\psi^{r-c}(z = \bar{z} = 0)| = 2.896$. When $\Omega = 2.3, \epsilon = 0.15, \theta = -\pi/4$, the peak value 3.116 occurs at $z = -0.005, \bar{z} = 0.0167$, while $|\psi^{r-c}(z = \bar{z} = 0)| = 3.108$. For $\theta = 0$, the peak value is $3 + \epsilon$, which occurs at $z = \bar{z} = 0$. Interestingly, $|\psi^{r-c}(z = \bar{z} = 0)| = 3 + \epsilon$ even for $\theta = \pi$.

The experimental observation of the surface elevation $\eta(x, t)$ in the rogue wave is described by Eqs. (19), (4), and (2).

Explicitly,

$$\eta(x,t) = \text{Re} \left[ia_0 e^{i(k_0 x - \omega_0 t - \frac{k_0^2 a_0^2 \omega_0}{2} t)} \left(1 - \epsilon C(x,t) + i \epsilon \frac{\sigma}{\Omega^2} S(x,t) - \frac{4 - 4ik_0^2 a_0^2 \omega_0 t - \epsilon \frac{16}{\Omega^2} \{C(x,t) - i \frac{\sigma}{\Omega^2} S(x,t)\} - \epsilon \frac{16}{\Omega^2} \sqrt{2} k_0^2 a_0 (x - c_g t) \{S(x,t) + i \frac{\sigma}{\Omega^2} C(x,t)\}}{1 - \epsilon \frac{4}{\Omega^2} C(x,t) + \{8k_0^4 a_0^2 (x - c_g t)^2 + k_0^4 a_0^4 \omega_0^2 t^2\} \{1 + \epsilon \frac{4}{\Omega^2} C(x,t) - \epsilon \frac{32}{\Omega^4} M(x,t) S(x,t)\}} \right) \right], \quad (20)$$

where

$$\begin{aligned} C(x,t) &= \cos \left(\sqrt{2} \Omega k_0^2 a_0 (x - c_g t) - \sigma \frac{k_0^2 a_0^2 \omega_0}{4} t + \theta \right), \\ S(x,t) &= \sin \left(\sqrt{2} \Omega k_0^2 a_0 (x - c_g t) - \sigma \frac{k_0^2 a_0^2 \omega_0}{4} t + \theta \right), \\ M(x,t) &= \sqrt{2} \Omega k_0^2 a_0 (x - c_g t) + \sigma \frac{k_0^2 a_0^2 \omega_0}{4} t. \end{aligned} \quad (21)$$

Figures 1 and 3 show plots for $\eta(x,t)$ in Eq. (20) with parameters $a_0 = 0.01$ m, $k_0 = 11.63$ m⁻¹, $\omega_0 = 10.7$ s⁻¹ (which are those of the experiment in [5]). We take $t \rightarrow t - 6$ and $a(x,t) \rightarrow ia(x,t)$ in Eq. (20) for comparison with the experimental curve in Fig. 1 (such that $0 < t < 12$), and the observation point is at $x = 0$.

Careful examination of Fig. 1 shows that there is a small concave in the amplitude for $1 < t < 3.5$ for both the solid and dashed lines, while the dotted line shows nearly constant amplitude. For $3.5 < t < 5$, both the solid and dashed lines drop sharply, while the dotted line shows a mild decrease. This phenomenon is most prominent at $t \sim 5$. The dashed line from the generalized Peregrine soliton fits the experimental data (solid line) better than the dotted line from the standard Peregrine soliton for $0 < t < 7$. The two theoretical curves (dashed and dotted) show discrepancies with the experimental data (solid line) for $t > 7$. Especially, the amplitude of the solid line seems locked for almost 1 s around $t \sim 8$. After that time, the solid line increases sharply for $9 < t < 10.5$. The dashed line shows the corresponding sharp increase for $8 < t < 9.5$, while the dotted line shows a mild increase at that time. For $t > 10.5$, the solid line starts developing a small concave, while the corresponding concave of the dashed line appears for $9.5 < t < 12$. The dotted line shows no such concave. It can be concluded that the generalized Peregrine soliton describes the rogue wave more accurately than the standard

Peregrine soliton. But the two theoretical curves cannot explain the locking behavior of the experimental data around $t \sim 8$.

Regarding the description of the fluctuating background, there could be two possible approaches: (i) the first one applies well when the fluctuations are developed from background irregularities which spread all over the region of wave propagation. The irregularities are, for example, the defects and/or refractive index changes spread all over the optical fiber or a variation of the water depth in the ocean in water waves. In this case, the fluctuating backgrounds (or noises) can be described by an equation which includes these irregularities and thus becomes some kind of generalized NLSE (the so-called inhomogeneous NLSE). (ii) The second one is for the cases where the irregularities are confined to some restricted regions or boundaries. Examples are the irregular paddle motion in the water tank experiment and a junction of two different refractive indices in the optical fiber. Then, the confined irregularities develop fluctuating waves, and these waves propagate to an adjacent “regular” region where there are no irregularities. In this case, one can use the standard NLSE and its solution to describe the propagation of fluctuations in the regular region. The propagating fluctuation is described by the cnoidal wave solution of the standard NLSE, which is ψ_0 in Eq. (8). ψ_0 in Eq. (5) is the approximate solution obtained from Eq. (8) by taking the small amplitude limit (see Secs. III C and III D).

In nature, we can expect both effects to be present simultaneously. In this case, the generalized Peregrine soliton of an inhomogeneous NLSE should describe the rogue wave with fluctuating backgrounds in an “irregular” region. But we can arrange the experimental environment such that rogue waves develop in the regular region. Especially, the constant

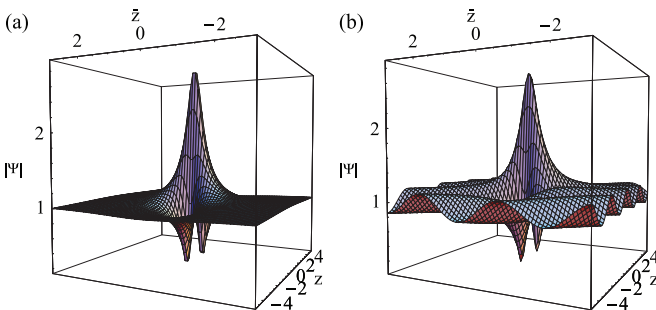


FIG. 2. (Color online) (a) The standard Peregrine soliton with $\epsilon = 0$ and (b) the generalized Peregrine soliton with the parameters $\epsilon = 0.15, \Omega = 2.3, \sigma = 2.61, \theta = -3\pi/4$.

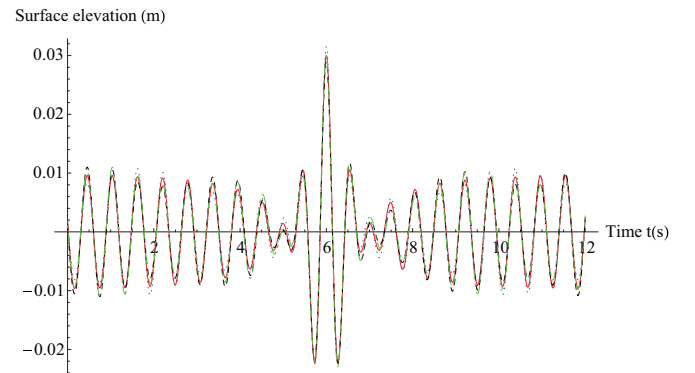


FIG. 3. (Color online) Surface height at $x = 0$. The standard Peregrine soliton with $\epsilon = 0$ (red solid line) and the generalized Peregrine soliton ($\theta = 0$ for the blue dotted line, $\theta = -\pi/2$ for the green dash-dotted line, and $\theta = -3\pi/4$ for the black dashed line) with the parameters $\epsilon = 0.15, \Omega = 2.3$ are shown.

depth and width of the water tank provide an ideal experimental environment for the regular region, which essentially has no irregularity. Then, the irregular paddle motion develops fluctuations, and they propagate through the water tank and develop a rogue wave. In this case, the generalized Peregrine soliton can describe many portions of the rogue wave better than the standard Peregrine soliton, as was seen in Fig. 1. However, the limited experimental data do not permit a concrete conclusion on the nature of irregularities.

In Fig. 3, the red solid line corresponds to the standard Peregrine soliton, obtained with $\epsilon = 0$. The blue dotted, green dash-dotted, and black dashed lines show the plots of the generalized Peregrine soliton, from Eq. (20), with $\theta = 0, -\pi/2$, and $-3\pi/4$, respectively (other common parameters are $\epsilon = 0.15, \Omega = 2.3, \sigma = 2.61$). The dotted line ($\theta = 0$) shows the fluctuating background and is symmetric with respect to time, as expected. The dashed and dash-dotted lines show asymmetry in time and fluctuating backgrounds, which are observed in the experiment in Fig. 1. The fluctuating background of the dashed line ($\theta = -\pi/2$) is shifted to the left

compared to that of the dash-dotted line ($\theta = -3\pi/4$). Thus agreements between experiments and theoretical predictions can be improved by suitably choosing the parameters: ϵ for the fluctuating width, Ω for the fluctuating period, and θ for the fluctuating phase.

Finally, a more refined description of the fluctuating background is possible with a generalized form of ψ_0 as follows:

$$\psi_0(z, \bar{z}) = -i \left[1 + \sum_{i=1}^N \epsilon_i \cos Y_i \right] e^{2i\bar{z} - i \sum_{i=1}^N \epsilon_i \frac{\sigma_i}{\Omega_i^2} \sin Y_i}, \quad (22)$$

where

$$Y_i = \Omega_i z + \sigma_i \bar{z} + \theta_i, \quad \sigma_i = \pm \Omega_i \sqrt{\Omega_i^2 - 4}, \quad (23)$$

and Ω_i, θ_i are arbitrary parameters. Summation on $i = 1, N$ means the fluctuation is described by the superposition of N cosine waves of different wavelengths and phases. All ϵ_i should be small. ψ_0 in Eq. (22) can have various forms of fluctuating backgrounds, including those of the *noisy* type. Then the corresponding Peregrine soliton is given by

$$\psi^{r-c}(z, \bar{z}) = i e^{2i\bar{z}} \left[1 - \sum \epsilon_i \cos Y_i + i \sum \epsilon_i \frac{\sigma_i}{\Omega_i^2} \sin Y_i - \frac{4 + 16i\bar{z} - \sum \epsilon_i \frac{16}{\Omega_i^2} (\cos Y_i + \Omega_i z \sin Y_i) - i \sum \epsilon_i \sigma_i \frac{16}{\Omega_i^2} (\Omega_i z \cos Y_i - \sin Y_i)}{1 - \sum \epsilon_i \frac{4}{\Omega_i^2} \cos Y_i + (4z^2 + 16\bar{z}^2)(1 + \sum \epsilon_i \frac{4}{\Omega_i^2} \cos Y_i) - \sum \epsilon_i \frac{32}{\Omega_i^2} (\Omega_i z - \sigma_i \bar{z}) \sin Y_i} \right]. \quad (24)$$

It was checked explicitly using MATHEMATICA that ψ_0 in Eq. (22) and ψ^{r-c} in Eq. (24) are approximate solutions of the NLSE (3) up to order $O(\epsilon_i)$.

Conclusively, defects and/or noisy boundaries confined to a finite region generate the fluctuating or noisy background. Then, it propagates and develops the rogue wave in the regular region. Under this scenario, the rogue wave resides on the fluctuating background and is described by the generalized Peregrine soliton.

[1] D. H. Peregrine, *ANZIAM J.* **25**, 16 (1983).
 [2] N. Akhmediev and E. Pelinovsky, *Eur. Phys. J. Spec. Top.* **185**, 1 (2010).
 [3] V. Ruban, Y. Kodama, M. Ruderman, J. Dudley, R. Grimshaw, P. V. E. McClintock, M. Onorato, C. Kharif, E. Pelinovsky, T. Soomere, G. Lindgren, N. Akhmediev, A. Slunyaev, D. Solli, C. Ropers, B. Jalali, F. Dias, and A. Osborne, *Eur. Phys. J. Spec. Top.* **185**, 5 (2010).
 [4] C. Finot, G. Millot, F. Dias, G. Genty, N. Akhmediev, B. Kibler, J. Fatom, and J. M. Dudley, *Nat. Phys.* **6**, 790 (2010).
 [5] A. Chabchoub, N. P. Hoffmann, and N. Akhmediev, *Phys. Rev. Lett.* **106**, 204502 (2011).
 [6] A. Chabchoub, N. P. Hoffmann, and N. Akhmediev, *J. Geophys. Res.* **117**, C00J02 (2012).
 [7] H. Bailung, S. K. Sharma, and Y. Nakamura, *Phys. Rev. Lett.* **107**, 255005 (2011).
 [8] V. E. Zakharov, *J. Appl. Mech. Tech. Phys.* **9**, 190 (1968).
 [9] M. Erkintalo, K. Hammani, B. Kibler, C. Finot, N. Akhmediev, J. M. Dudley, and G. Genty, *Phys. Rev. Lett.* **107**, 253901 (2011).
 [10] M. J. Ablowitz and P. A. Clarkson, *Solitons, Nonlinear Evolution Equations and Inverse Scattering*, London Mathematical Society Lecture Note Series (Cambridge University Press, Cambridge, 1991).
 [11] H. J. Shin, *J. Phys. A* **45**, 255206 (2012).
 [12] H. J. Shin, *Phys. Rev. E* **69**, 067602 (2004).
 [13] V. Matveev and M. Salle, *Darboux Transformations and Solitons*, Springer Series in Nonlinear Dynamics (Springer, Heidelberg, 1990).